

Supporting Information

pH-Guided Self-assembly of Copper Nanoclusters with Aggregation-Induced Emission

*Xuxian Su and Jinbin Liu**

Key Laboratory of Functional Molecular Engineering of Guangdong Province, School of Chemistry and Chemical Engineering, South China University of Technology, Guangzhou 510640, China

Corresponding Author

*Jinbin Liu, Email: cejbliu@scut.edu.cn

Materials and equipment

L-cysteine, copper (II) chloride monohydrate ($\text{CuCl}_2 \cdot \text{H}_2\text{O}$), bovine serum albumin (BSA), sodium chloride (NaCl) and L-ascorbic acid (Vc) were obtained from Sangon Biotech (Shanghai, China). Glucose oxidase (GOx), D-(+)-glucose, glycine and fluorescein were obtained from Sigma-Aldrich (Shanghai, China). Potassium chloride (KCl) and α -laltose were purchased from Kermel (Tianjin, China). D-fructose and maltose were obtained from Shanghai Bo'ao Biological Technology Co., Ltd. (Shanghai, China). Hydrogen peroxide (H_2O_2), cucrose, disodium hydrogen phosphate dodecahydrate ($\text{Na}_2\text{HPO}_4 \cdot 12\text{H}_2\text{O}$) and potassium dihydrogen phosphate (KH_2PO_4) were purchased from Guangzhou Chemical Reagent Factory (Guangzhou, China). Sephadex G25 was purchased from Solarbio (Beijing, China). 3-Hydroxypicolinic acid (3-HPA) was purchased from J&K Scientific Ltd. (Beijing, China). Sodium hydroxide (NaOH) and hydrochloric acid (HCl) were purchased from Zhi Yuan reagent Co., Ltd. (Tianjin, China). Nitric acid (HNO_3) was purchased from Enox (Jiangsu, China). Solutions of K^+ , Na^+ , Ca^{2+} , Zn^{2+} , and Fe^{3+} were prepared from KCl, NaCl, CaCl_2 , $\text{Zn}(\text{Ac})_2$ and $\text{Fe}(\text{NO}_3)_3$, respectively. All chemicals were used without further purification. All glassware was cleaned with fresh aqua regia ($\text{HCl}/\text{HNO}_3 = 3:1$, V/V) before use.

Luminescence spectra were recorded on a LS 55 luminescence spectrophotometer (PerkinElmer, USA) using 10 nm/10 nm slit widths for both excitation and emission measurements. FT-IR spectra were collected from 400 to 4000 cm^{-1} using a TENSOR 27 Fourier transform infrared (FT-IR) spectrometer (Bruker, Germany). The X-ray photoelectron spectroscopy (XPS) measurements were performed using a ESCALAB 250Xi instrument (Thermo Scientific, UK) with Al $K\alpha$ X-ray radiation (1486.6 eV) as excitation source, and C1s (284.8 eV) was used as reference energy for all binding energies. The photoluminescence quantum yields (QYs) were measured directly with the absolute QY measurement system C11347-11 (Hamamatsu Photonics K. K., Japan), equipped with an excitation light source and monochromator, an integrating sphere capable of nitrogen gas flow and a CCD spectrometer for detecting the whole spectral range simultaneously. This instrument was calibrated with fluorescein (QY, 88%) before the measurements. **Atomic force microscope (AFM) was carried out on a**

FSM-Nanoview 1000 (FSM-Precision, Suzhou) in tapping mode equipped with MikroMasch NSC11 AFM tip. Transmission electron microscopy (TEM) was carried out on a JEOL JEM 2100F TEM (Japan) with an accelerating voltage of 200 kV. Scanning electron microscope (SEM) was performed on a MERLIN compact field-emission SEM (Germany). The powder structure of the CuNCs was characterized by X-ray Diffraction (XRD) using a Biller D8 Advance XRD instruments, and the value of 2 theta was in between 30 degrees to 80 degrees. Matrix-Assisted Laser Desorption/Ionization Time of Flight Mass Spectrometry (MALDI-TOF MS) measurements were performed on a Bruker Daltonics Autoflex III Smartbean MALDI-TOF MS (Germany). The spectra were collected in positive-ion mode using 3-HPA (3-Hydroxypicolinic acid) as matrix. Elemental analyzer was carried out on a Vario EL cube (Elementar, Germany).

Experimental section

Sample preparations for AFM, TEM and SEM imaging

A typical sample for AFM imaging was prepared by spotting 40 μL sample onto a freshly cleaved mica surface after treatment with 1.0 M MgCl_2 . The mica substrate was tilted carefully to let the droplet to spread evenly on the mica surface. The sample droplet was removed after 1 minute, and then rinsed with 100 μL MgCl_2 (1 mM). The mica surface was completely dried with compressed air before imaging. All AFM images were processed with a freely available software: WSxM 5.0 Develop 8.1 (www.nanotec.es).¹

As for the TEM imaging, the prepared sample with a volume of 5 μL was spotted onto a copper grid supported carbon film. The excess sample was removed with a small piece of filter paper after 2 min. TEM imaging was performed on a JEM-2100F field emission TEM. As for the SEM imaging, 5 μL sample solution was dropped into a cleaned silicon wafer, and dried on the air. The samples on the silicon wafer were then sputtered with a thin layer of gold before the imaging with a MERLIN compact field-emission SEM.

X-ray Photoelectron Spectroscopy (XPS)

A piece of freshly cut aluminum foil ($1 \times 1 \text{ cm}^2$ square) was dropped 10 μL sample solution, and the sample was air-dried on the surface of aluminum foil at room temperature. This sample deposition process could be repeated several times to ensure enough sample loading. All obtained spectra were fitted with a mixed Gaussian-Lorentzian function by XPSPEAK 4.1 (a freeware).

Elemental analysis

Elemental analysis showed that the CuNCs aggregates were composed of 18.17 % C, 6.80 % N and 15.38 % S. Chemical formulas of cysteine-CuNCs can be expressed as Cu_xL_y , wherein L=L-cysteine containing a deprotonated thiol group ($\text{C}_3\text{H}_6\text{NO}_2\text{S}$, 120.01 g/mol), x =number of Cu atom, y =number of cysteine. The average ratio of Cu-to-cysteine= x/y . The calculations of the ratios (x/y) from C, N and S elements were listed as follows:

1. Calculation of x/y using the measured mass fraction of C:

$$18.17 \% = \frac{3y\text{Mr}_C}{(x\text{Mr}_{\text{Cu}} + y\text{Mr}_L)}, \text{ and } x/y = 1.35;$$

2. Calculation of x/y using the measured mass fraction of N:

$$6.80 \% = \frac{y\text{Mr}_N}{(x\text{Mr}_{\text{Cu}} + y\text{Mr}_L)}, \text{ and } x/y = 1.23;$$

3. Calculation of x/y using the measured mass fraction of S:

$$15.38 \% = \frac{y\text{Mr}_S}{(x\text{Mr}_{\text{Cu}} + y\text{Mr}_L)}, \text{ and } x/y = 1.39;$$

4. Calculation of average the ratio of Cu-to-cysteine (x/y):

$$(1.35 + 1.23 + 1.39) / 3 = 1.32.$$

Supplementary Data

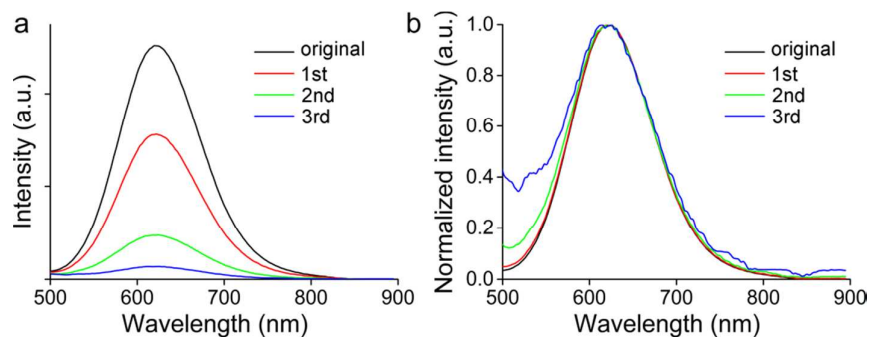


Figure S1. The Luminescence spectra (a) and normalized luminescence spectra (b) of the CuNC aggregates after washing for 3 times to remove the randomly hybrid cluster might be generated in the aggregated system.

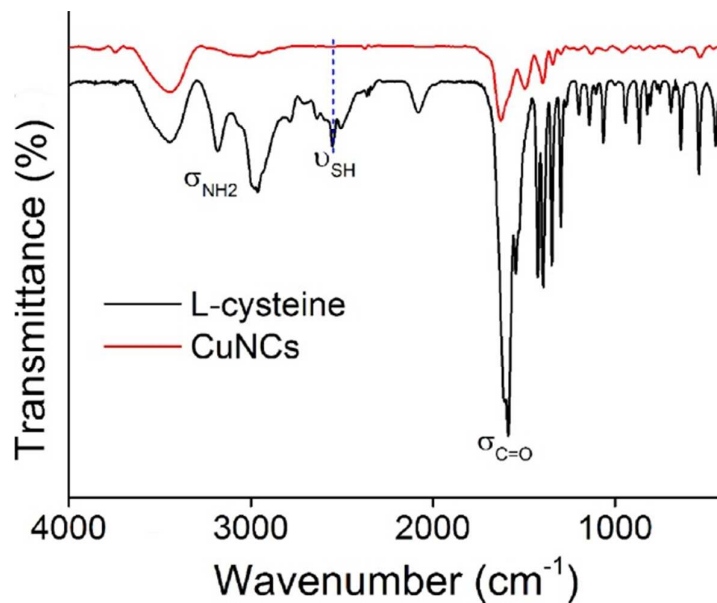


Figure S2. The FT-IR spectra of L-cysteine (black) and CuNC aggregates (red), respectively. The disappearance of the S-H stretching vibration peak at 2550 cm^{-1} from cysteine in the CuNCs demonstrated the formation of Cu-S bond between cysteine and CuNCs.

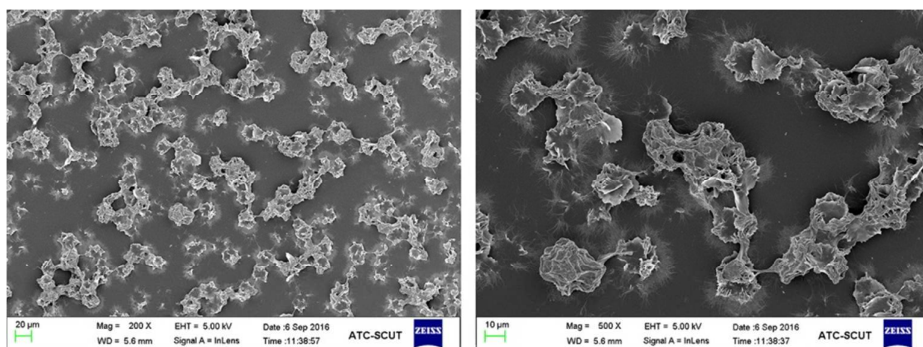


Figure S3. Typical SEM images of the synthesized CuNC aggregates (pH 3.0).

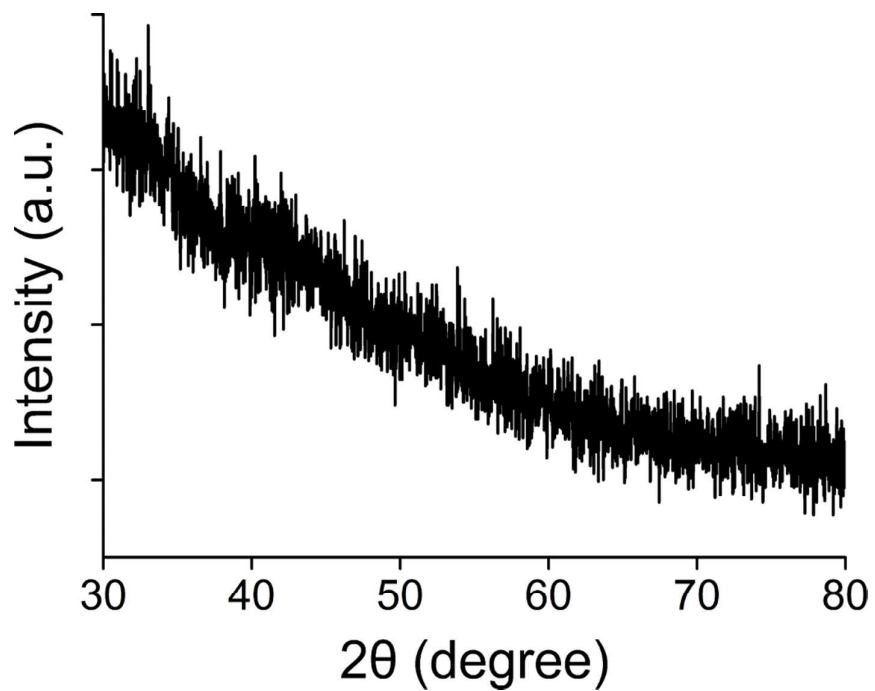


Figure S4. XRD spectra of the synthesized CuNC aggregates.

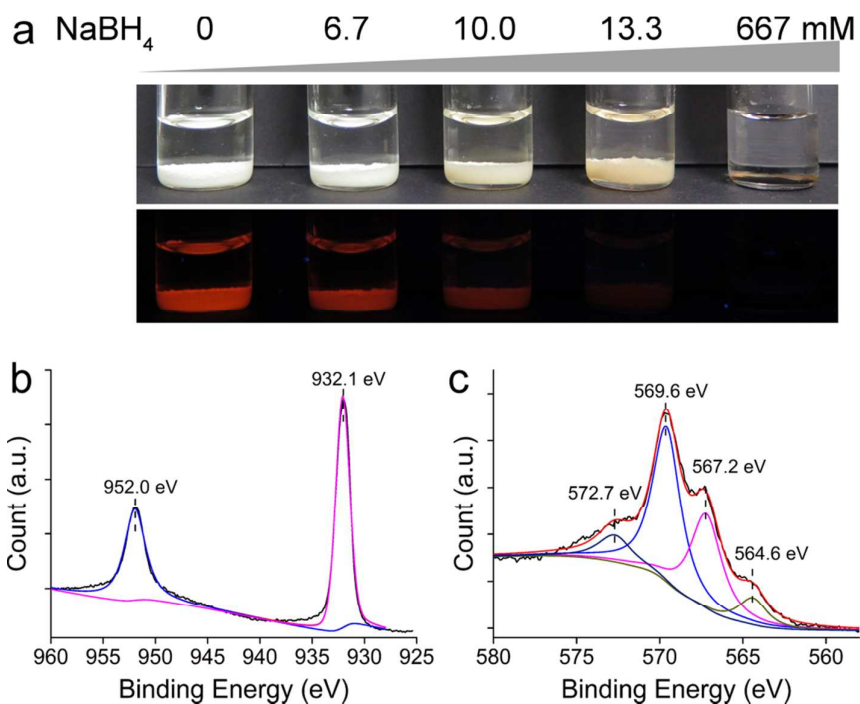


Figure S5. a) Photographs of the CuNC aggregates further reduced by NaBH₄ at different concentrations (from left to right: 0, 6.7 mM, 10.0 mM, 13.3 mM, 667 mM) after aging overnight at room temperature. The pictures were taken under room light (upper panel) and 365 nm UV light (lower panel), respectively. b) XPS of Cu 2p spectrum in CuNC aggregates that were reduced by NaBH₄ (667 mM) with no satellite peak observed, evidencing the absence of Cu (II) species. c) Peak fitted Cu LMM Auger spectrum for the reduced CuNC aggregates showing that the molar ratio of Cu(I)/Cu(0) was increased to 1:0.56.

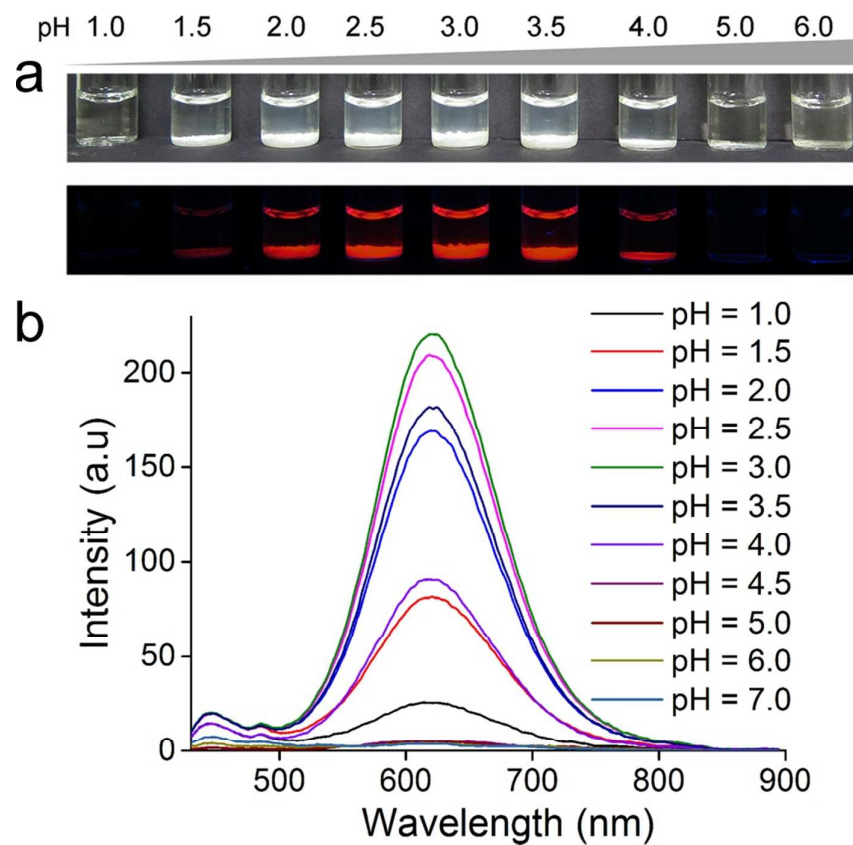


Figure S6. a) The photographs of the CuNC aggregates in PBS buffer at different pH values under room light (upper panel) and 365 nm UV light (lower panel), respectively. b) Luminescence spectra of CuNC aggregates in PBS buffer at different pH values.

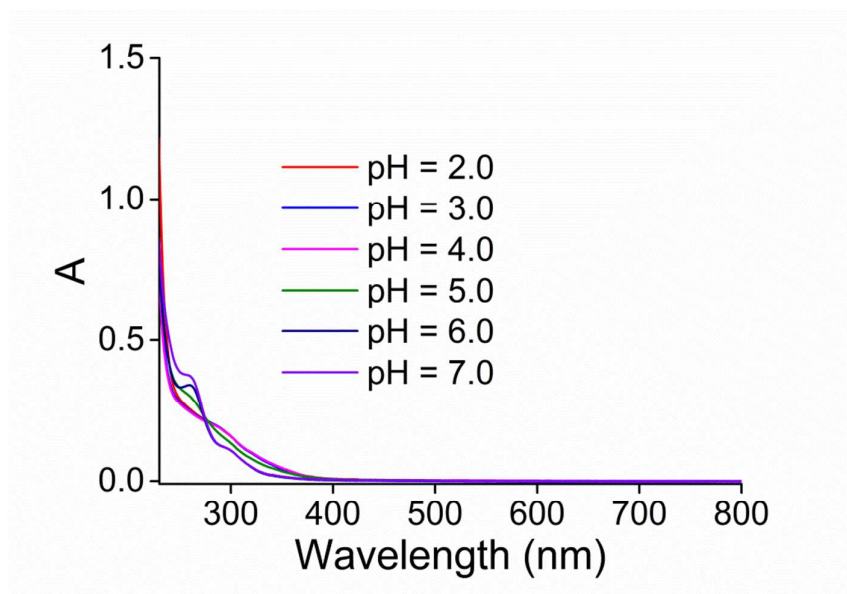


Figure S7. UV-Vis spectra of CuNC aggregates in PBS buffer at different pH values.

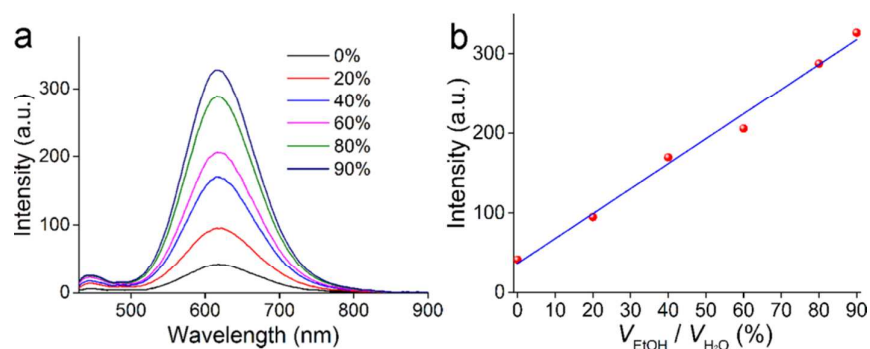


Figure S8. a) Luminescent spectra of CuNCs in mixed solvents of ethanol (EtOH) and water at pH 5.0 with different ratios of $V_{\text{EtOH}}/V_{\text{H}_2\text{O}}$ (0%, 20%, 40%, 60%, 80% and 90%). b) Plot of the luminescence intensities at 620 nm at pH 5.0 over different ratios of $V_{\text{EtOH}}/V_{\text{H}_2\text{O}}$. The emission intensity of the CuNCs (pH 5.0) increased with the increase of the amount of EtOH, demonstrating the AIE behaviour of synthesized CuNCs.

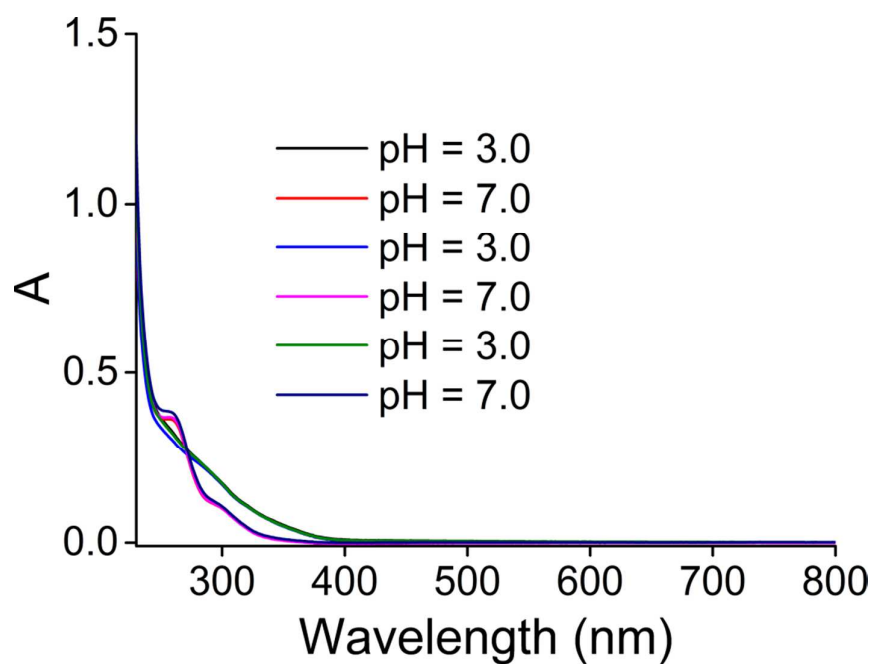


Figure S9. Reversibility of the absorbance spectra of the CuNCs between pH 3.0 and 7.0.

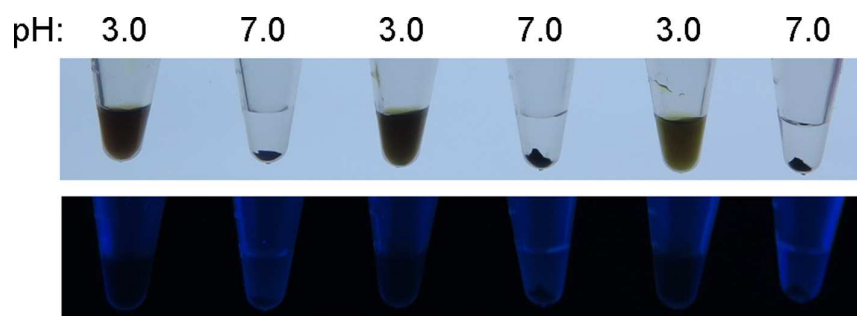


Figure S10. The reversible pH response of the CuNCs reduced by NaBH_4 (667 mM). The pictures were taken under room light (upper panel) and 365 nm UV light (lower panel), respectively.

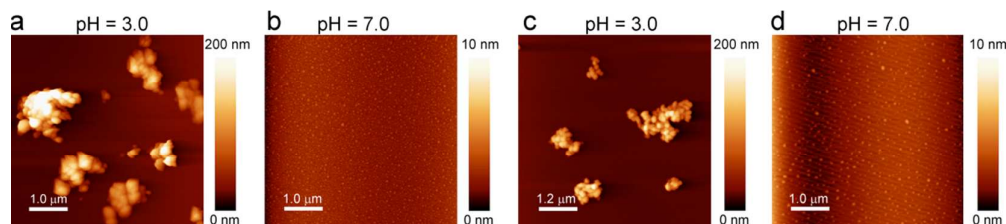


Figure S11. Reversibility of the structures of the CuNCs between pH 3.0 (a, c) and 7.0 (b, d), indicating that the structures of the CuNCs were also pH reversible.

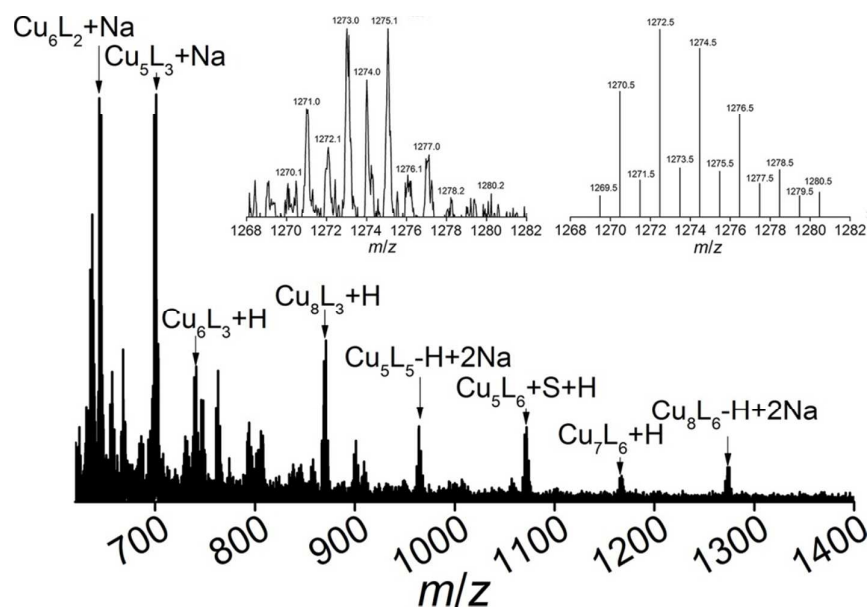


Figure S12. Positive mode MALDI-TOF MS analysis of synthesized CuNCs (pH 7.0) (where L stands for $C_3H_6NO_2S$). It showed that the highest m/z peak was assigned to $[Cu_8L_6-H+2Na]^+$. The lower mass peaks are ascribed to $[Cu_6L_2+Na]^+$, $[Cu_5L_3+Na]^+$, $[Cu_6L_3+H]^+$, $[Cu_8L_3+H]^+$, $[Cu_5L_5-H+2Na]^+$, $[Cu_5L_6+S+H]^+$ and $[Cu_7L_6+H]^+$, respectively. Inset: Experimental (right panel) and simulated isotopic (left panel) pattern of $[Cu_8L_6-H+2Na]^+$. The base peak at 1273.0 was perfectly in agreement with the theoretical exact mass of 1272.5 (deviation: 0.5). The observed isotope pattern matched well with the theoretical prediction.

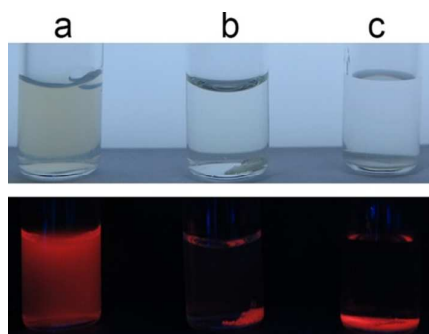


Figure S13. The comparison of pH-guided mild strategy and sonication-aided dispersion method in the fabrication of BSA/CuNCs hybrid nanostructures. (a) The BSA/CuNCs hybrid nanostructures made from pH-guided strategy; (b) The BSA/CuNCs hybrid nanostructures made from sonication-aided dispersion in the present of BSA; (c) The mixture of BSA and CuNC aggregates without pH adjustment or sonication. All the samples were subjected to centrifugation at 2000 g for 1 min and taken under room light (upper panel) and 365 nm UV light (lower panel). The results indicated that the hybrid nanostructures fabricated by the pH-guided strategy was much more stable than those made from sonication-aided dispersion. As showed in the results that the luminescence of the CuNC aggregates decreased after 30 min sonication, the CuNC aggregates would be partially degraded after a long time of sonication.

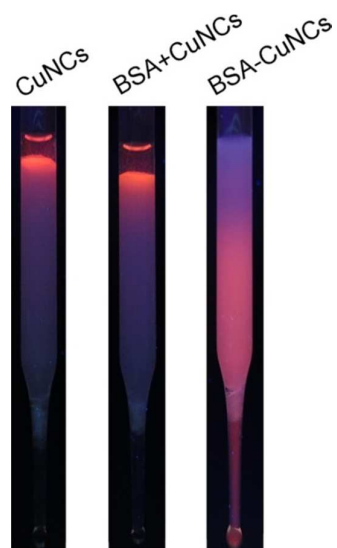


Figure S14. Purification of the BSA/CuNCs hybrid nanostructures with sephadex G25 column. The photographs of the sephadex G25 columns loading with samples of CuNC aggregates (left), mixture of BSA and CuNC aggregates (middle) and BSA/CuNCs hybrid nanostructures (right) were taken under 365 nm UV light. The BSA/CuNCs fabricated from the pH-guided strategy could pass through the sephadex G25 column, in sharp contrast to the BSA-free macroscopical CuNC aggregates or the mixture of BSA and CuNC aggregates that were trapped on the top of the sephadex G25 column due to their bulky sizes, demonstrating the success formation of the BSA/CuNCs hybrid nanostructures.

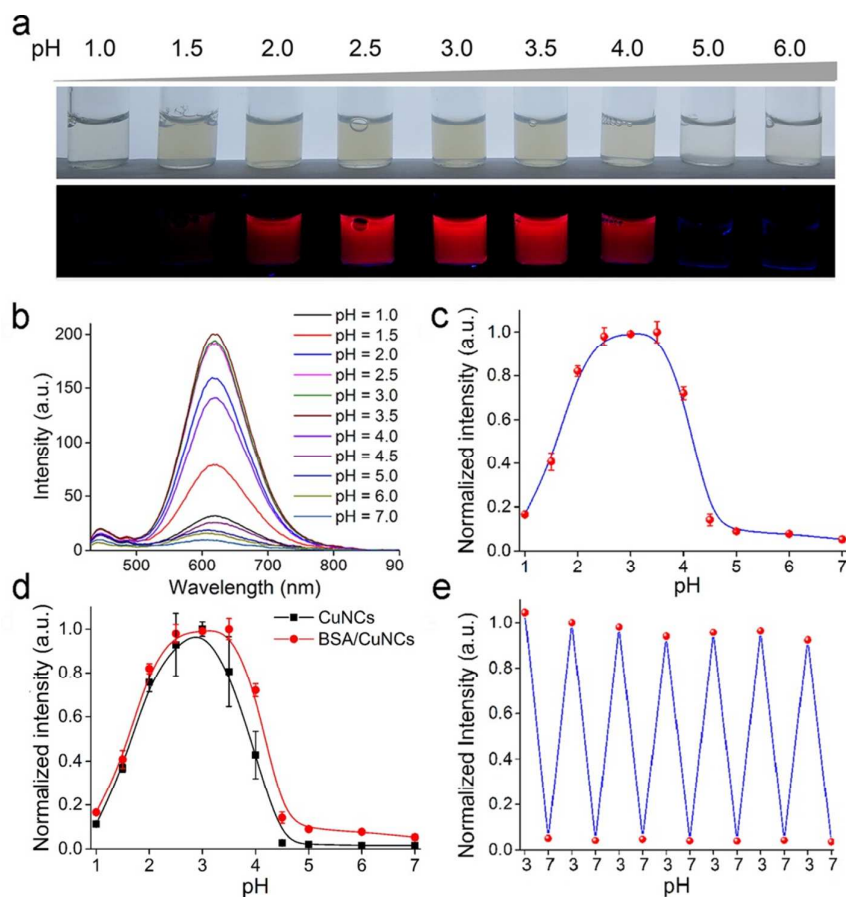


Figure S15. a) Photographs of the BSA/CuNCs hybrid nanostructures in PBS buffer at different pH values under room light (upper panel) and 365 nm UV light (lower panel), respectively. b) Luminescence spectra of the BSA/CuNCs hybrid nanostructures in PBS buffer at different pH values. c) Plot of the luminescence intensities (at 620 nm) over different pH values. d) Comparison of the luminescence intensities (at 620 nm) over different pH values of BSA-free CuNCs and BSA/CuNCs hybrid nanostructures, respectively. e) Reversibility of the pH-dependent emission of the BSA/CuNCs hybrid nanostructures between pH 3.0 and pH 7.0, demonstrating the BSA/CuNCs hybrid nanostructures were highly stable.

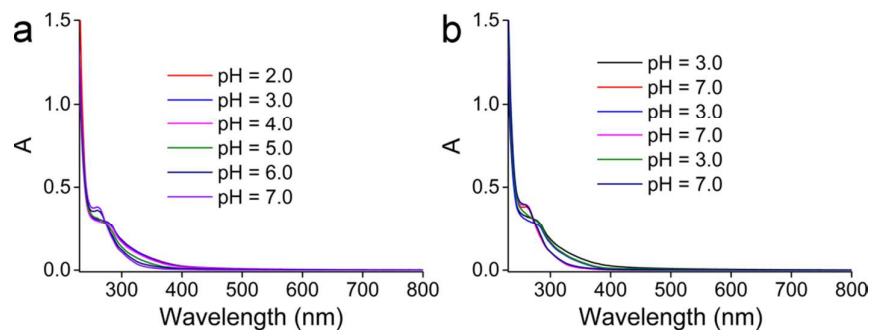


Figure S16. a) UV-Vis spectra of BSA/CuNCs in PBS buffer at different pH values. b) Reversibility of the absorbance spectra of the BSA/CuNCs between pH 3.0 and 7.0.

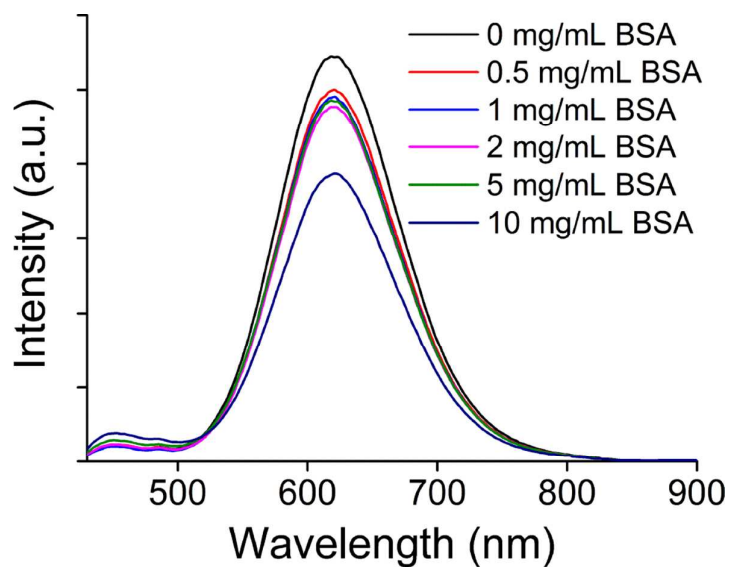


Figure S17. The luminescence spectra of the BSA/CuNCs hybrid nanostructures assembled at different concentrations of BSA (pH=3.0).

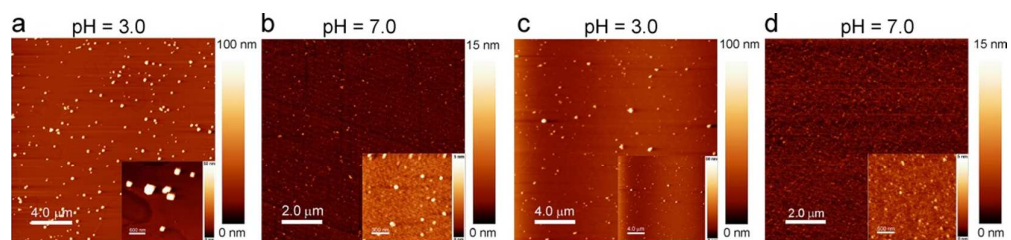


Figure S18. Reversibility of the structures of the BSA/CuNCs between pH 3.0 (a, c) and 7.0 (b, d), indicating the structures of the BSA/CuNCs were also pH reversible.

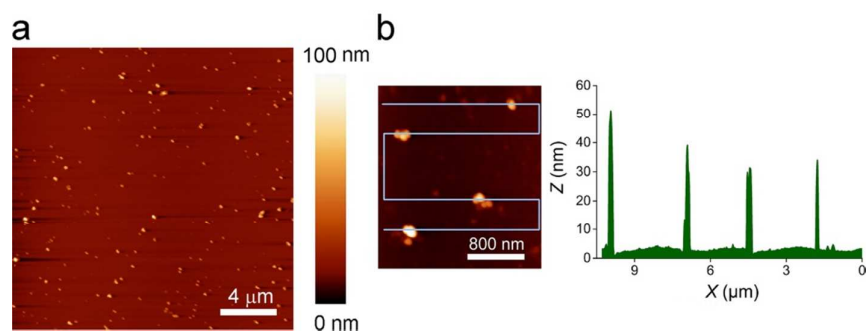


Figure S19. a) AFM images of the GOx/CuNCs hybrid nanostructures (pH 3.0) and b) the height profile analysis of AFM images showing that the average height of the hybrid nanostructure was ~ 30 nm.

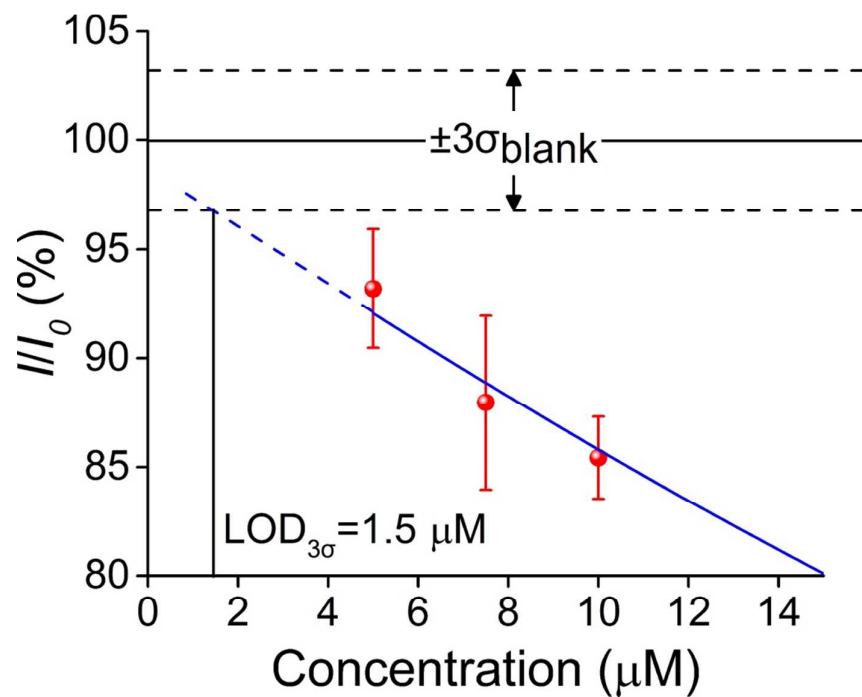


Figure S20. A magnified graph of the above calibration curve of glucose concentrations (5, 7.5 and 10 μM) showed the limit of detection (LOD, 3δ) was 1.5 μM.

Table S1. Comparison of the copper nanomaterial-based methods for the determination of glucose

Materials ^a	Method ^b	Detection range (μM)	LOD (μM)	Time	Ref.
CuNC–CNTs-GRE	E	0.7-3,500	0.21	5 s	2
Cu ₂ O/GNs	E	300-3,300	3.3	9 s	3
Cu@Cu ₂ O NS-NW	E	0.7-20,000	0.04	0.1s	4
BSA-CuNCs	A	10-1,000	100	15 min	5
DPA-CuNCs	F	50-2,000	10	4 hour	6
PEI-CuNCs	F	10-100	8	45 min	7
GOx/CuNCs	F	5-100	1.5	40 min	This method

^a CNTs carbon nanotubes, GRE glassy carbon electrode, CuNCs copper nanoclusters, GNs graphene nanosheets, NWs nanowires, NSs nanosheets. PEI polyethyleneimine, BSA bovine serum albumin, D-PA D-penicillamine

^b F fluorescence, E electrochemistry, A absorbance

References:

- (1) Horcas, I.; Fernández, R.; Gómez-Rodríguez, J. M.; Colchero, J.; Gómez-Herrero, J.; Baro, A. M., WSXM: A Software for Scanning Probe Microscopy and a Tool for Nanotechnology. *Rev. Sci. Instrum.* **2007**, *78* (1), 013705.
- (2) Kang, X.; Mai, Z.; Zou, X.; Cai, P.; Mo, J., A Sensitive Nonenzymatic Glucose Sensor in Alkaline Media with a Copper Nanocluster/multiwall Carbon Nanotube-modified Glassy Carbon Electrode. *Anal. Biochem.* **2007**, *363* (1), 143-50.
- (3) Liu, M.; Liu, R.; Chen, W., Graphene Wrapped Cu₂O Nanocubes: Non-enzymatic Electrochemical Sensors for the Detection of Glucose and Hydrogen Peroxide with Enhanced Stability. *Biosens. Bioelectron.* **2013**, *45*, 206-12.
- (4) Zhao, Y.; Fan, L.; Zhang, Y.; Zhao, H.; Li, X.; Li, Y.; Wen, L.; Yan, Z.; Huo, Z.,

- Hyper-Branched Cu@Cu₂O Coaxial Nanowires Mesh Electrode for Ultra-Sensitive Glucose Detection. *ACS Appl. Mater. Interfaces* **2015**, 7 (30), 16802-12.
- (5) Hu, L.; Yuan, Y.; Zhang, L.; Zhao, J.; Majeed, S.; Xu, G., Copper Nanoclusters as Peroxidase Mimetics and Their Applications to H₂O₂ and Glucose Detection. *Anal. Chim. Acta* **2013**, 762, 83-6.
- (6) Jia, X.; Yang, X.; Li, J.; Li, D.; Wang, E., Stable Cu Nanoclusters: From an Aggregation-induced Emission Mechanism to Biosensing and Catalytic Applications. *Chem. Commun.* **2014**, 50 (2), 237-9.
- (7) Ling, Y.; Zhang, N.; Qu, F.; Wen, T.; Gao, Z. F.; Li, N. B.; Luo, H. Q., Fluorescent Detection of Hydrogen Peroxide and Glucose with Polyethyleneimine-templated Cu Nanoclusters. *Spectrochim. Acta. Part A* **2014**, 118, 315-20.